# Adsorption mode of the chiral modifier cinchonidine on Au(111)

**ARTICLE** *in* APPLIED SURFACE SCIENCE · JANUARY 2007

Impact Factor: 2.71 · DOI: 10.1016/j.apsusc.2006.07.084

Available online at www.sciencedirect.com
ScienceDirect
Applied Surface Science 253 (2007) 3480–3484
applied surface science
www.elsevier.com/locate/apsusc

# Adsorption mode of the chiral modifier cinchonidine on Au(1 1 1)

B. Behzadi [a,b], D. Ferri [b], A. Baiker [b], K.-H. Ernst [a,*]

[a] *Empa, Swiss Federal Laboratories for Materials Testing and Research, Überlandstrasse 129, CH-8600 Dübendorf, Switzerland*
[b] *Institute for Chemical and Bioengineering, Department of Chemistry and Applied Biosciences, ETH Zurich, Hönggerberg, HCI, CH-8093 Zürich, Switzerland*

Received 10 April 2006; accepted 17 July 2006
Available online 7 September 2006

**Abstract**

The adsorption of the chiral modifier cinchonidine on Au(l 1 1) in UHV has been studied by means of TPD, LEED and XPS. In the monolayer the molecule is bound via nitrogen lone pair electrons of its quinoline part rather than via the π-system of this aromatic moiety. Intact molecular desorption is only observed for the multilayers. Decomposition in the first monolayer upon heating occurs above 400 K, indicating a stronger interaction in the monolayer. No long-range ordered structures were observed via LEED. Long-time exposure leads to rearrangement and further stabilization of the first molecular monolayer. Quinoline is bound to gold via the nitrogen lone pair as well. The binding energy of 9.6 kcal/mol is characteristic for physisorption.


*PACS:* 68.43.−h; 82.65.−s

*Keywords:* Chirality; Enantioselective heterogeneous catalysis; Cinchonidine; Quinoline; Chiral modifier; Au(1 1 1)

## 1. Introduction

There is an increasing demand for enantiomerically pure compounds in chemical and pharmaceutical industry. In this respect, heterogeneous enantioselective catalysis is a sustainable approach to chiral compounds. By coadsorbing a chiral modifier on a catalytically active metal surface, an enantiomeric bias is introduced. Most prominent enantiospecific reactions are hydrogenation of α-functionalized ketones on cinchona-modified platinum group metal catalysts and hydrogenation of β-keto carboxylic acid esters and ketones on tartaric acid-modified nickel catalysts [1,2]. The modifier influences the alignment of the reactant so that identical enantiotopic faces are turned towards the surface. This relative alignment of the prochiral species then determines the direction of hydrogen attack and thus, the handedness of the product. The metal surface serves as active site and provides anchoring of the modifier.

Beyond this basic picture, the underlying mechanism of enantioselective surface chemistry is still debated. The present understanding is that enantioselectivity is induced by a 1:1 interaction between chiral modifier and reactant [3]. No ordered structures have been observed for CD on Pt [4]. Long-range ordered structures of the modifier species tartaric acid (TA) and CD have only been reported on copper surfaces [5–7], but these are catalytically inactive with respect to hydrogenation. Chiral voids in enantiomorphous lattice structures have been proposed as enantioselective adsorption sites [8], and the homochiral alignment of methylacetoacetate (MAA) in an ordered coadsorbed (*R*,*R*)-TA structure on Ni(1 0 0) has been shown directly in STM [9]. Long-range order, however, was also blamed for low enantioselectivity by suppressing the required equimolar reactant-modifier interaction [10].

These examples show that for more insight on the surface enantioselectivity mechanism, the local adsorption geometry of the modifier and the long-range structure on the surface has to be determined. Moreover, rational design of chiral catalyst systems requires control of the adsorption mode of the modifier. The lack of stability of a highly selective chiral heterogeneous catalyst is actually the main drawback and the reason that only few systems are available today. One approach must be therefore the generation of stable chiral surface systems with catalytic activity. The local adsorption geometry may change with coverage of modifier and reactant or with impurity concentration as well as temperature, leading to dramatic

* Corresponding author. Tel.: +41 44 823 43 63; fax: +41 44 823 40 34.
*E-mail address:* karl-heinz.ernst@empa.ch (K.H. Ernst).

0169-4332/$ – see front matter 
doi:10.1016/j.apsusc.2006.07.084

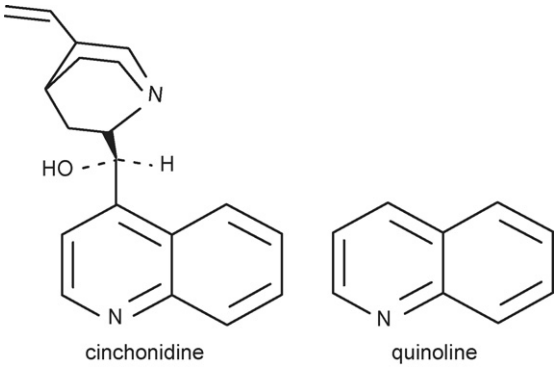


Fig. 1. Structural formula of cinchonidine (CD) and quinoline. In CD an aliphatic ring system (quinuclidine) is connected via a hydroxy methylene group to the aromatic quinoline part.

changes in enantioselectivity [11]. For example, CD on Pt forms three different adsorbate species with increasing coverage [12,13], while for CD on Pd only two species were found [14]. On both metals at low coverage, a parallel orientation of the quinoline aromatic ring system (Fig. 1) with respect to the surface plane is favoured. A tilted geometry is preferred at higher coverage, whereby the binding occurs via the electron lone pair of the quinoline part. At medium coverage, a α-quinolyl species, in which a hydrogen atom is abstracted from an aromatic ring, has been observed on Pt as well [12]. Very recently further insight into the rich conformational behaviour of cinchonidine on Pt(1 1 1) was gained by DFT calculations. Eight conformationally different adsorption states of cinchonidine were identified and their possible role as chiral sites in the enantioselective hydrogenation of α-ketoesters has been discussed in light of the currently existing experimental evidence [15].

There are many examples that bimetallic catalysts substantially enhance selectivity [16]. Baddeley and coworkers introduced this idea to the enantioselective hydrogenation on tartrate-modified Ni(1 1 1)/Au substrates [17,18]. We recently transferred this idea to the cinchonidin/Pt and cinchonidin/Pd catalysts and characterized these model systems with XPS, AFM and ATR-IR studies of adsorbed CO as probe molecule [19]. For the reference system CD/Au, ATR-IR showed that CD is adsorbed with the quinoline tilted with respect to the surface plane [20].

The aim of this work was to gather information on the monolayer structure using *in vacuo* experimental techniques like LEED, XPS and TPD. Most important objectives of this study were long-range order, chemical structure and local geometric structure. In order to identify which nitrogen atom of CD interacts with the surface, we also studied quinoline on Au(1 1 1) as a reference system.

## 2. Experimental

Experiments have been carried out in a stainless steel ultra-high vacuum (UHV) chamber ($p = 2 \times 10^{-10}$ mbar) equipped with facilities for temperature programmed desorption (TPD), low energy electron diffraction (LEED), and X-ray photoelectron spectroscopy (XPS). The sample could be resistively heated to 1000 K and liquid-nitrogen cooled to about 80 K. Preparation of the Au(1 1 1) (MateK, roughness $< 0.1$ μm) surface was achieved by standard UHV procedures (Ar bombardment and annealing) and controlled by XPS and LEED, the latter showing the $\left(22 \times \sqrt{3}\right)$ structure before CD adsorption. This preparation was also applied after every TPD experiment. (*R*8,*S*9)-cinchonidine (Fluka 98.95%) deposition was performed with a homemade Knudsen cell held at 120 °C during sublimation. The relative coverage has been controlled via XPS by normalization of the C 1s peak to the Au 4d substrate signal. Quinoline (Aldrich $\geq$ 99%) has been further purified by freeze-pump-thaw cycles prior to the adsorption experiments. Exposure of the Au crystal held at 80 K to quinoline has been performed by back-filling the chamber with quinoline partial pressures between $1 \times 10^{-8}$ mbar and $1 \times 10^{-7}$ mbar. TPD spectra were acquired with a linear heating rate of 4.1 K/s. XPS-energy calibration, usually achieved by assigning the Au 4f 7/2 peak to 84 eV, has been done here by setting the highest intensity C 1s component (obtained via peak fitting) to 285 eV. This procedure has been chosen in order to account for local electrostatic charging effect due to three-dimensional island growth.

## 3. Results and discussion

Prior to evaluation of local bonding geometry and lateral long-range order, we calibrated the amount necessary to form a complete CD monolayer via TPD. The most important results are presented in Figs. 2 and 3. Fig. 2 shows peaks that are indicative for molecular desorption. The most intensive fragment in the mass spectrometer at $m/z = 136$ represents the aliphatic quinuclidine fragment of CD. With the sample held at room temperature (RT), already after 30 s exposure a peak at 340 K became detectable. However its intensity did not further increase substantially, even at 50 times higher doses.

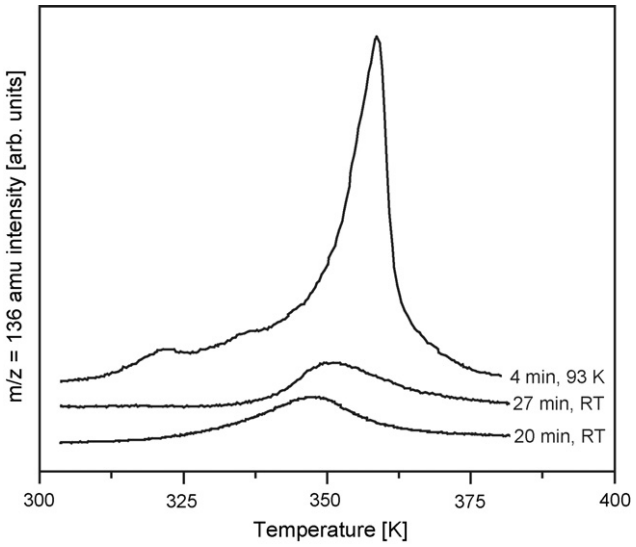


Fig. 2. Molecular desorption measured via the fragment mass 136 (quinuclidine part of CD) from multilayered films. The strong dependence on substrate temperature indicates a high desorption rate at RT.

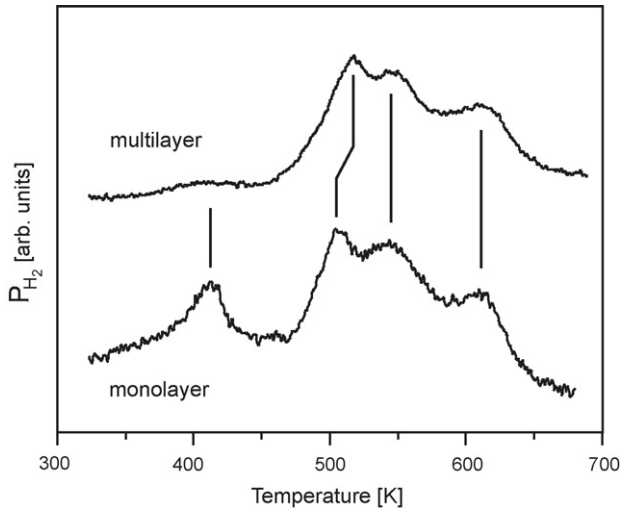


Fig. 3. Hydrogen evolution from a cinchonidine monolayer (15 s dose) and from multilayers (30 min). The change of decomposition pathway indicates a rearrangement in the monolayer after prolonged dosing.

Fig. 2 further shows the effect on molecular desorption by increasing the exposure from 20 min to 27 min. Cooling the substrate, on the other hand, increased the intensity of molecular desorption dramatically, even at much smaller doses. This observation must be explained by a relatively high desorption rate from the second layer at RT, i.e., a low sticking probability for CD on CD. Hence the molecule–substrate interaction is much stronger than the molecule–molecule interaction. However, multiplayer growth at RT is observed after very large doses. Apparently, second layer nucleation and growth has to overcome a critical size of nuclei (Ostwald ripening).

Hydrogen desorption signals after exposures of 30 s and 30 min are shown in Fig. 3. The hydrogen evolves from the thermally induced decomposition of CD on the gold surface. Despite the large difference in exposure, no substantial changes in signal area are observed. It is important to mention that intact CD in the first monolayer at RT on Pt(1 1 1) has been observed via ToF-SIMS [21]. Hence, one can safely assume that CD is intact at RT on gold as well. Taking the first appearance of molecular desorption after 30 s into account, we conclude that (i) after 30 s the monolayer is saturated, (ii) no molecular desorption takes place from the first monolayer, and (iii) the molecule undergoes thermally induced decomposition at relatively high temperatures on the gold surface. However, going from short to long time exposure, a decomposition peak observed at 410 K almost disappears and a peak at 505 K shifts by 10 K to higher temperature, while the decomposition steps at 545 K and 610 K do not change with exposure. We assign this observation to a rearrangement of the monolayer during prolonged CD exposure. Under steady second layer adsorption–desorption conditions, the first layer slowly rearranges towards higher stability, and two of the decomposition reactions become higher activated due to this rearrangement. Since the Au surface is believed to play an active role in all decomposition steps, we conclude that this rearrangement increases the stability by enhanced supra- or supermolecular interactions in the molecular layer, more suppressing the interaction of reactive molecular groups with the substrate. However, we were not able to find any superstructure in LEED for different coverages and temperatures. The thermal stability effect must be therefore assigned to a local rearrangement, either in the single adsorbate complex or between adjacent molecules, but not within a long-range lattice structure.

In contrast to CD, no decomposition of quinoline has been observed here via TPD, i.e., mass 2 and mass 129 peaks appear at the same temperature (not shown here). From the smallest doses on, molecular desorption has been observed at 161 K from the gold surface. With increasing exposure this peak shifts to higher temperatures (max. 170 K) and a second desorption peak evolves at 180 K, with the peak maximum then shifting to above 200 K. The peak shape of this second peak is typical for zero order desorption kinetics indicating desorption from the multilayer. The low desorption temperature here stands clearly for physisorption. A rough estimate, based on first order desorption kinetics after the Readhead formula [22], delivers a value of 9.6 kcal/mol, in excellent agreement with the 9.1 kcal/mol resulting from DFT calculations for tilted or perpendicular adsorption geometry [20].

Information on chemical states in the monolayer has been obtained via XPS. The most important feature is presented in Fig. 4, showing the N 1s signals after different doses of CD and quinoline. Basically two peaks are observed for all species and

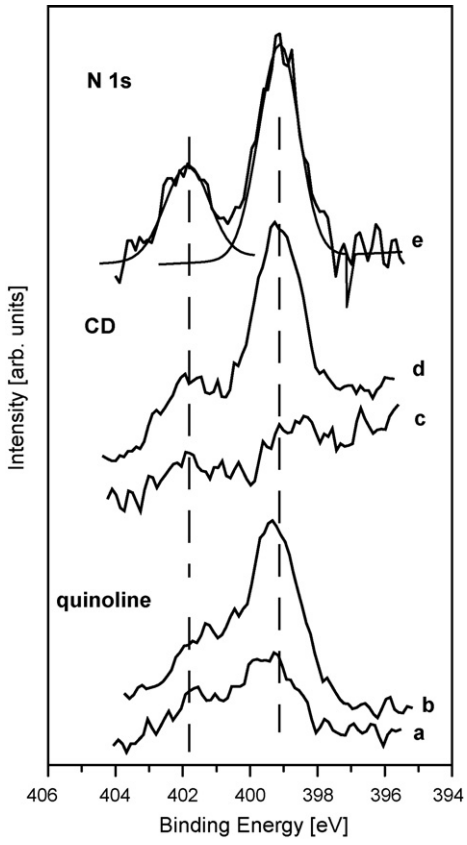


Fig. 4. N 1s XPS signals of quinoline (a: 0.06 L; b: 0.6 L) and CD (c: 1 min dose; d and e: 20 min dose). Spectrum e has been acquired with higher energy resolution (lower analyzer pass energy) for peak fitting.

all coverages. Fitting Gaussian peaks under a spectrum acquired with higher resolution for CD gives N 1s binding energies of 399.2 eV and 401.8 eV. The values for quinoline are similar. Both peaks appear at low coverage simultaneously. The high energy peak gets saturated quickly while for multilayer conditions only the low energy peak is increased in intensity.

For undistorted aromatic sp2- or aliphatic sp3-hybridized nitrogen, peaks at 399.0–399.8 eV are characteristic [23]. N 1s signals at around 402 eV, however, are an indication for positively charged nitrogen. With the aromatic ring system bound via the π-electron system in a parallel geometry to the surface, we would not expect such strong shift in N 1s binding energy, since the interaction would be spread over the 10 atoms of the aromatic system (nine carbon and one nitrogen). For quinoline on Pt(1 1 1) this has been confirmed previously [24]. A charge transfer from the quinoline nitrogen to the gold substrate explains the higher N 1s binding energy. For N-containing aromatic molecules, a tilted or perpendicular geometry is quite common, e.g. bisquinoline and 8-hydroxyquinoline on silver and gold nanoparticles were found to interact via the N-electron lone pair to the substrate [25]. For pyridine on various Ni, Cu, Ag, Au, Pt and Ru surfaces, this geometry has been found as well [26,27]. In analogy to the high coverage situation on Pd and Pt, CD is therefore expected to bind to Au via the quinoline nitrogen lone-pair orbital, leading to the tilted adsorbate geometry. The fact that we see a similar chemical shift for quinoline supports this conclusion. Since ATR-IR measurements of CD on Au in $CH_2Cl_2$ show a tilted quinoline group [20], we assume that in UHV a similar bonding configuration is present. In contrast to Pt and Pd, the bonding to Au via the aromatic ring is too weak to force the molecule into a parallel adsorption mode, and the bulky aliphatic group at the aromatic ring systems puts a steric constrain to the parallel orientation. This scenario is further supported by DFT calculation of quinoline on Au(1 1 1) destabilizing the parallel configuration by 3 kcal/mol [20]. However, adsorbate complexes of pyridine, lepidine or dihydro-CD on Pt(1 1 1) [4,24], for example, do not show such a strong chemical shift, even when the interaction to the substrate via the N electron lone pair occurs. The same observation has been made for the amino group of naphtylethylamine directly interacting with the Pt surface [10]. On the other hand, it has been shown for pyrazine ($C_4H_4N_2$), that the N 1s binding energy on Au(1 1 1) is larger than on Ag(1 1 1) [28]. When pyrazine changed its alignment from parallel to perpendicular to the Au(1 1 1) surface, an additional peak shift from 399.4 eV to 400.2 eV has been reported [28]. However, the two different nitrogen atoms in the perpendicular configuration were not resolved so that only an average value was determined. In addition the chemical shift for the N bound to the surface is expected to be substantially lower than for quinoline due to an electronic mesomeric effect induced by the second N atom in position 4, pointing away from the surface. Without the second nitrogen in the aromatic ring, the positive charge on the nitrogen bound to the substrate must be higher and a larger chemical shift, as observed here, is expected.

After the 30 min CD exposure at RT (Fig. 4d and e), the coverage is just slightly above one monolayer and only the low-energy N 1s peak grows further in intensity with increasing coverage. Therefore, both nitrogen atoms, i.e., in the quinoline and the quinuclidine group in the multilayer show a signal at around 399 eV. For quinoline, the 399.3 eV peak intensity increases for doses above 0.6 L (Fig. 4b), but the 401.8 eV peak intensity remains the same. Again, the low energy peak can be assigned either to the multilayer quinoline not in contact with the gold surface or to a parallel adsorbed molecule. Taking into account, that quinoline is stronger bound via the N-lone pair electrons even at small coverage, and that the low energy peak is substantially increased in the multilayer regime, we assign the low energy peak to quinoline which is not in direct contact with the gold surface. Because it is also observed at initial adsorption, we further conclude that quinoline clusters into 3D islands on gold even at smallest coverage. Up to a dose of 0.6 L the clusters grow in two- and three-dimensions, and both N 1s peaks are increased simultaneously, until above 0.6 L only the ''3D peak'' keeps growing. This means that the intermolecular acting forces, most probably π–π interactions, prevail over molecule substrate interaction. This is experimentally confirmed here by the shift of the TPD signal to higher temperature with increasing coverage.

Finally, we briefly discuss the fact that quinoline is only physisorbed, while CD undergoes decomposition. A stronger adsorption for CD than for quinoline on gold has been observed by ATR-IR experiments in $CH_2Cl_2$ [20]. Apparently further interaction, either with the surface or between the CD molecules stabilizes CD substantially. However, the XPS analysis delivers similar electronic bonding conditions for CD and quinoline. But it does not necessarily reflect the situation close to decomposition. The molecule may transfer to a different geometry, and a rearrangement in the monolayer has indeed been observed via the change of the hydrogen desorption signal. Note that due to its rotational flexibility CD can form an intramolecular hydrogen bond between separate hydroxyl group and the quinuclidine nitrogen lone pair orbital. For steric reasons, a second N–Au bond of the quinuclidine N is not possible. The tilted or perpendicular oriented aromatic system allows two strong intermolecular hydrogen bonds between OH and N and a π–π interaction between the aromatic moieties. However, we would expect a long-range ordered structure for such arrangement. On the other hand, the rather weak bond to the surface and stronger intermolecular acting forces will lead to 3D clustering from the beginning on, not allowing long range order.

## 4. Conclusions

Cinchonidine interacts with Au(1 1 1) via the nitrogen of the quinoline group and has therefore an adsorption geometry in which the aromatic part is tilted or perpendicular with respect to the surface plane. Although weakly bound, the charge transfer from the nitrogen to the gold is pronounced. In this configuration, quinoline is physisorbed and desorbs intactly upon heating. CD, however, undergoes decomposition in the monolayer, most probably due to strong lateral intermolecular interaction, stabilizing the monolayer.

## Acknowledgement

Financial support by the Schweizerischer Nationalfonds is gratefully acknowledged.

## References

[1] A. Baiker, Catal. Today 100 (2005) 159.
[2] C.J. Baddeley, Top. Catal. 25 (2003) 17.
[3] T. Bürgi, A. Baiker, Acc. Chem. Res. 37 (2004) 909.
[4] A.F. Carley, M.K. Rajumon, M.W. Roberts, P.B. Wells, J. Chem. Soc., Faraday Trans. 91 (1995) 2167.
[5] M. Ortega Lorenzo, S. Haq, T. Bertrams, P. Murray, R. Raval, C.J. Baddeley, J. Phys. Chem. B 103 (1999) 10661.
[6] Q.-M. Xu, D. Wang, L.-J. Wan, C.-L. Bai, Y. Wang, J. Am. Chem. Soc. 124 (2002) 14300.
[7] Q.-M. Xu, D. Wang, M.-J. Han, L.-J. Wan, C.-L. Bai, Langmuir 20 (2004) 3006.
[8] M. Ortega Lorenzo, C.J. Baddeley, C. Muryn, R. Raval, Nature 404 (2000) 376.
[9] T.E. Jones, C.J. Baddeley, Surf. Sci. 519 (2002) 237.
[10] J.M. Bonello, F.J. Williams, R.M. Lambert, J. Am. Chem. Soc. 125 (2003) 2723.
[11] T. Bürgi, A. Baiker, J. Am. Chem. Soc. 120 (1998) 12920.
[12] D. Ferri, T. Bürgi, J. Am. Chem. Soc. 123 (2001) 12074.
[13] D. Ferri, T. Bürgi, A. Baiker, Chem. Commun. (2001) 1172.
[14] D. Ferri, T. Bürgi, A. Baiker, J. Catal. 210 (2002) 160.
[15] A. Vargas, A. Baiker, J. Catal. 239 (2006) 220.
[16] C.T. Campbell, Ann. Rev. Phys. Chem. 44 (1990) 775.
[17] T.E. Jones, T.C.Q. Noakes, P. Bailey, C.J. Baddeley, J. Phys. Chem. B 108 (2004) 4759.
[18] T.E. Jones, T.C.Q. Noakes, P. Bailey, C.J. Baddeley, Surf. Sci. 569 (2004) 63.
[19] B. Behzadi, D. Ferri, P. Kappenberger, R. Hauert, K.-H. Ernst, A. Baiker, in preparation.
[20] B. Behzadi, A. Vargas, D. Ferri, K.-H. Ernst, A. Baiker, J Phys Chem B 110 (2006) 17082–17089.
[21] B. Behzadi, P. Rossbach, D. Ferri, A. Baiker, K.-H. Ernst, unpublished results.
[22] P.A. Redhead, Vacuum 12 (1962) 203.
[23] J.F. Moulder, W.F. Stickle, P.E. Sobol, K.D. Bomben, in: J. Chastain, King, Jr. (Eds.), Handbook of X-ray Photoelectron Spectroscopy, 2nd ed., Physical Electronics, Inc., Eden Prairie, 1995.
[24] J.M. Bonello, R.M. Lambert, Surf. Sci. 498 (2002) 212.
[25] S. Kim, S.-W. Joo, Vib. Spectrosc. 39 (2005) 74.
[26] W.-B. Cai, L.-J. Wan, H. Noda, Y. Hibino, K. Ataka, M. Osawa, Langmuir 14 (1998) 6992.
[27] C.I. Smith, A.J. Maunder, C.A. Lucas, R.J. Nichols, P. Weightman, J. Electrochem. Soc. 150 (2003) E233.
[28] U.W. Hamm, V. Lazarescu, D.M. Kolb, J. Chem. Soc. Faraday Trans. 92 (1996) 3785.